TECHNICAL NOTE

Cytometry PART A
Journal of the International Society for Advancement of Cytometry

MIFlowCyt

High Throughput FRET Analysis of Protein–Protein Interactions by Slide-Based Imaging Laser Scanning Cytometry

Nikoletta Szalóki,[1] Quang Minh Doan-Xuan,[1] János Szöllősi,[1,2] Katalin Tóth,[3] György Vámosi,[1]* Zsolt Bacsó[1]*

[1]Department of Biophysics and Cell Biology, Medical and Health Science Center, Research Center for Molecular Medicine, University of Debrecen, Nagyerdei krt. 98, H-4032, Debrecen, Hungary

[2]HASc-UD Cell Biology and Signaling Research Group, Medical and Health Science Center, University of Debrecen, Hungary

[3]German Cancer Research Center (DKFZ), Biophysics of Macromolecules (B040), Im Neuenheimer Feld 580, D-69120, Heidelberg, Germany

Received 26 January 2012; Revision Received 24 April 2013; Accepted 12 May 2013

This article is dedicated to the memory of Dr. Robert Clegg, a pioneer and leading expert in FRET techniques.

Grant sponsor: Országos Tudományos Kutatási Alap; Grant numbers: K77600, K103965, NK 101337, K75752, CK78179; Grant sponsor: New Hungary Development Plan—European Social Fund—European Regional Development Fund; Grant numbers: TAMOP-4.2.1/B-09/1/KONV-2010-0007, TAMOP-4.2.2.A-11/1/KONV-2012-0023 "VÉD-ELEM" Project, TAMOP-4.2.2.A-11/1/KONV-2012-0025; Grant sponsor: Baross Gábor Program; Grant number: REG_EA_09-1-2009-0010; Grant sponsor: Magyar Ösztöndíj Bizottság—Deutscher Akademischer Austausch Dienst; Grant numbers: MÖB/47-1/2010, MÖB/21-1/2013

• Laser scanning cytometry (LSC) is a slide-based technique combining advantages of flow and image cytometry: automated, high-throughput detection of optical signals with subcellular resolution. Fluorescence resonance energy transfer (FRET) is a spectroscopic method often used for studying molecular interactions and molecular distances. FRET has been measured by various microscopic and flow cytometric techniques. We have developed a protocol for a commercial LSC instrument to measure FRET on a cell-by-cell or pixel-by-pixel basis on large cell populations, which adds a new modality to the use of LSC. As a reference sample for FRET, we used a fusion protein of a single donor and acceptor (ECFP-EYFP connected by a seven-amino acid linker) expressed in HeLa cells. The FRET efficiency of this sample was determined via acceptor photobleaching and used as a reference value for ratiometric FRET measurements. Using this standard allowed the precise determination of an important parameter (the alpha factor, characterizing the relative signal strengths from a single donor and acceptor molecule), which is indispensable for quantitative FRET calculations in real samples expressing donor and acceptor molecules at variable ratios. We worked out a protocol for the identification of adherent, healthy, double-positive cells based on light-loss and fluorescence parameters, and applied ratiometric FRET equations to calculate FRET efficiencies in a semi-automated fashion. To test our protocol, we measured the FRET efficiency between Fos-ECFP and Jun-EYFP transcription factors by LSC, as well as by confocal microscopy and flow cytometry, all yielding nearly identical results. Our procedure allows for accurate FRET measurements and can be applied to the fast screening of protein interactions. A pipeline exemplifying the gating and FRET analysis procedure using the CellProfiler software has been made accessible at our web site.

• **Key terms**
fluorescence resonance energy transfer; FRET; laser scanning cytometry; high throughput; protein–protein interactions

Fluorescence or Förster resonance energy transfer (FRET) is a nonradiative process, in which energy is transferred from an excited fluorescent donor dye to a neighboring acceptor within its 2–10 nm vicinity by dipole–dipole coupling (1). In order for FRET to take place, the emission spectrum of the donor should overlap with the absorption spectrum of the acceptor, and the two dyes should have a proper relative orientation (2,3). The process is characterized by the FRET efficiency, E, which is the probability that a donor in the excited state transfers its energy to a nearby acceptor. E depends on the 6th power of the separation distance, R, between the donor and the acceptor:

$$E = \frac{1}{1+(R/R_0)^6}, \quad (1)$$

where R_0 is the Förster radius, at which $E = 0.5$. Because of its sensitive distance dependence, FRET can be used as a molecular ruler to assess intra- or inter-molecular distances (4), molecular conformation or association state. FRET has several effects on the fluo-

Additional Supporting Information may be found in the online version of this article.
Nikoletta Szalóki and Quang Minh Doan-Xuan are equal first authors.
György Vámosi and Zsolt Bacsó are equal senior authors.

Correspondence to: György Vámosi, Department of Biophysics and Cell Biology, Medical and Health Science Center, Research Center for Molecular Medicine, University of Debrecen, 98 Nagyerdei krt., H-4032 Debrecen, Hungary. E-mail: vamosig@med.unideb.hu and Zsolt Bacsó, Department of Biophysics and Cell Biology, Medical and Health Science Center, Research Center for Molecular Medicine, University of Debrecen, 98 Nagyerdei krt., H-4032 Debrecen, Hungary. E-mail: bacso@med.unideb.hu

Published online 10 July 2013 in Wiley Online Library (wileyonlinelibrary.com)

DOI: 10.1002/cyto.22315

rescence parameters of the donor and the acceptor, which can be used to determine E in different ways (3,5,6). The fluorescence lifetime and quantum yield of the donor decreases resulting in a decrease of the donor intensity (donor quenching), whereas the intensity of the acceptor is enhanced (sensitized emission). E can also be determined by selectively bleaching the donor (7,8) or the acceptor. In acceptor photobleaching, the enhancement of the donor intensity is measured after photodestruction of the acceptor dye (9,10). The advantage of photobleaching methods is the simplicity of the experiment and data analysis. However, irreversible photobleaching precludes monitoring the time course of processes on the same cells. Bleaching requires time, which can lead to the motion of the sample compromising the spatial resolution. Reversible blinking of fluorescent proteins, especially of red variants such as mRFP1 and mCherry, is another source of complications in photobleaching experiments.

Ratiometric methods are faster and nondestructive (11,12). They are based on the simultaneous detection of donor quenching and acceptor sensitized emission at multiple wavelengths. By using spectral and instrumental correction factors, pure donor and acceptor intensities (proportional to the expression levels) and FRET efficiencies can be derived on a cell-by-cell or pixel-by pixel basis by using flow cytometry or imaging microscopy. The flow cytometric version of the method provides excellent statistics over large cell populations (11,13,14), while microscopic imaging allows FRET analysis of adherent cells with sub-cellular resolution and in a repetitive manner in situ. A limitation of intensity based FRET methods is that they cannot resolve donor subpopulations characterized by different individual E values, e.g., those having or missing an acceptor pair. Thus, the measured apparent E value is an average over individual FRET efficiencies arising from different donors in the observation area (e.g., in a diffraction limited spot). In case only a fraction of donors is in complex with an acceptor, the gained FRET efficiency can be considered as a lower limit of the real E value. To resolve donor subpopulations characterized by different E values, fluorescence lifetime measurements (15–17) or single molecule conditions are needed (18,19).

Cyan and yellow fluorescent proteins (ECFP and EYFP), as well as green and red fluorescent proteins (EGFP and mRFP1 or mCherry), are often used as donor–acceptor pairs because of their substantial spectral overlap and their consequently high R_0 (20–22). Earlier, we used EGFP- and mRFP1 or mCherry to map interactions between FP-tagged nuclear or plasma membrane proteins using ratiometric FRET measurements by flow cytometry and confocal laser scanning microscopy (CLSM) (23,24). A pivotal problem of ratiometric FRET methods is the determination of the so-called α factor, which is a "photon exchange rate" comparing signal intensities in the donor and transfer detection channels arising from equal amounts of excited donor and acceptor dyes. To assess α, fusion proteins of donor and acceptor dyes can be used, which are expressed in a single polypeptide at one-to-one ratio (23,24).

Fos and Jun proteins are members of the bZIP family of transcription factors containing a highly conserved basic region involved in DNA binding and a heptad repeat of leucine residues. They function as homo- or hetero-dimers that bind to AP-1 (activator protein-1) regulatory elements in the promoter and enhancer regions of numerous mammalian genes (25). Because of their propensity to form stable heterodimers via a leucine-zipper, Fos and Jun are often used as positive controls in dimerization studies. Earlier, we demonstrated their stable heterodimer formation by FCCS (26) and FRET (23) in live cells, and described the C-terminal conformation of the complex using a Fos-GFP + Jun-mRFP1 pair.

The laser scanning cytometer (LSC) is a microscope-based cytofluorometer, which has attributes of both flow cytometry and microscopy (27). LSC expands the capabilities of flow cytometry to the analysis of solid tissues and adherent cells and significantly improves the statistic power of microscopy methods. Optical signals from fluorophore or dye labeled individual cells lodged on a microscope slide are measured at multiple wavelengths (28,29). The specimen carrier is mounted on a computer-controlled, motor-driven stepper stage allowing automated analysis of thousands of individual cells in a short duration. Detected signals comprise forward light scattering, light-loss, and fluorescence intensities. Contouring by one or a combination of these signals allows segmentation of the image, e.g., discrimination of cells or cellular organelles. From the primary signals, the total fluorescence, highest pixel intensity, or total area of a cell or a sub-cellular structure can be determined, and arithmetic calculations among parameters can be carried out. LSC is capable of relocalizing cells allowing, e.g., monitoring the same cells before and after a treatment or following the time course of processes. LSC has been found useful to analyze various cellular processes ranging from enzyme reaction kinetics to apoptotic DNA damage (30–33).

The phenomenon of FRET donor de-quenching has been used in some applications. Enhancement of donor emission

after photobleaching the acceptor moiety of FRET-based tandem dyes has been demonstrated (34). Cleavage by caspase of a CFP-YFP-labeled FRET sensor has been detected in an apoptosis assay (35). However, the FRET efficiency has not been assessed in any of these applications, and no quantitative FRET measurements have been carried out to investigate molecular associations; the focus of the aforementioned studies was different.

Here, we demonstrate that a commercially available standard LSC equipped with 405-, 488-, and 633-nm laser lines can be used for the identification of adherent, ECFP-EYFP double-positive HeLa cells. It is shown that ECFP and EYFP fluorescence can be detected with sufficiently high sensitivity and accuracy, and application of a reference sample with known FRET efficiency makes reliable FRET measurements on other samples possible. We compare FRET results obtained with a CLSM having optimal excitation wavelengths for the excitation of ECFP and EYFP (458 and 514 nm) with results gained from the LSC and a flow cytometer, both having suboptimal excitation wavelengths (405 and 488 nm). We introduce a novel numerical method to calculate the so-called α factor and the FRET efficiency from the same set of equations simultaneously. By using an ECFP-EYFP fusion protein as a standard, FRET efficiencies measured between Fos and Jun proteins using the different instruments are nearly identical. We define the methodology for semi-automated FRET measurements uniting the high throughput of flow cytometric FRET with the capability of subcellular resolution and cell back-tracking in a single instrument. Our method can facilitate screening of protein interactions by using FRET-based LSC assays.

Materials and Methods

Cell Culture, Plasmid Construction, Transfection, and Fluorescence Labeling

Cell culture conditions, transfection, and fluorescence labeling are described in the Supporting Information. Shortly, FRET experiments were carried out using HeLa cells transfected with fluorescent proteins. Construction of the expression vectors pSV-c-Fos-ECFP, pSV-c-Jun-EYFP, and the positive control, pSV-ECFP-EYFP (coding for the fusion of the two fluorescent proteins connected by a RNPPVAT linker) is described elsewhere (26). pSV-Fos^{215}-ECFP is a truncated version of full-length Fos-ECFP, where the last 164 amino acids have been deleted (23). Cells co-transfected with ECFP and EYFP plasmids were used as a negative control for FRET. Cells transfected with ECFP or EYFP alone were used for the determination of spectral cross-talk of the dyes between detection channels. For measurements with LSC and confocal microscopy, cells were plated in μ-Slide 8-well Ibidi chambered coverslip (Ibidi GmbH, Planegg/Martinsried, Germany). Membrane proteins were stained with Cy5 succinimidyl ester to define cell contours for segmentation of LSC data.

Laser Scanning Cytometric FRET

For slide-based scanning, an iCys Research Imaging Cytometer (CompuCyte Corporation, Westwood, MA) was used. The instrument is based on an Olympus IX-71 inverted microscope equipped with three lasers, photodiodes (detecting light loss and scatter) and four photomultiplier tubes (PMTs). A 405-nm solid state laser, a 488-nm Argon laser, and a 633-nm HeNe laser were alternatively operated in multitrack mode to excite ECFP, EYFP, and Cy5, respectively. Laser beams scanned the sample point by point. The autofocus utility determined the inclination of the cover slip by triangulation (based on reflection of the 488-nm laser). During the scan, a fixed offset from the bottom of the cover slip was applied, which placed the focus to the middle plane of cells. User-defined areas on the specimen having optimal cell density were marked as regions of interest (ROIs) and scanned in an automated process. Each ROI was automatically divided into smaller areas called scan fields by the software. Each scan field (1024 $\times$ 768 pixels) was scanned by a focused laser beam via an oscillating mirror in the y direction and by the motorized stage in the x direction with a step size of 0.25 μm. The arising fluorescence signals were collected via a 40$\times$ (NA 0.75) objective, whereas transmitted light was captured by the light loss detector. Laser intensities at the objective were 151 μW for the 405-nm and 27 μW for the 488-nm lines. Donor and transfer signals with an excitation at 405 nm were collected through 460–500 and 520–580 nm band-pass filters by separate PMTs; the acceptor was excited at 488 nm and detected at 520–580 nm by the same PMT as the transfer signal; Cy5 fluorescence was excited at 633 nm and detected through a 650-nm long-pass filter. Raw scanned images were processed post-acquisition by the CellProfiler software, in which cellular events were defined, and pixel-by-pixel FRET calculations were carried out according to equations described in the "Data Analysis" section. FRET efficiencies were also calculated on a cell-by-cell basis from the mean cellular intensities gained from the ImageProfiler software by using Microsoft Excel for $n \sim 500$ cells for each sample. Photostability of the dyes was checked by a time lapse experiment where the sample was scanned seven times. The extent of bleaching between two consecutive scans was 1% and 2.8% for ECFP and EYFP (Supporting Information Fig. S1).

Flow Cytometric FRET

Flow cytometric FRET measurements were carried out on a FACSAria III instrument (Becton Dickinson, San Jose, CA). Forward and side scattering were used to gate out debris and apoptotic cells. Donor and transfer signals were excited by a 405-nm solid state laser and detected between 430–470 and 515–545 nm, whereas the acceptor signal was excited by a 488-nm solid state laser and measured between 515 and 545 nm. Because of the spatial separation between the laser foci, fluorescence signals excited by the two lasers were detected with a time delay minimizing spectral crosstalk. For FRET calculations from flow cytometric data, the Reflex software developed at our institute was used (36). FRET efficiencies were presented as mean values of $\sim$10,000 double positive cells.

Collection of Ratiometric FRET Data by Confocal Laser Scanning Microscopy

FRET measurements were performed on a Zeiss LSM 510 confocal microscope (Carl Zeiss, Jena, Germany) equipped with a 63× Plan Apochromat oil immersion objective (NA 1.4). The donor and transfer signals were excited by the 458-nm line of an Argon ion laser and detected simultaneously between 475–525 nm and 530–600 nm; the acceptor signal was excited at 514 nm and detected between 530 and 600 nm. The intensities of the 458-nm and 514-nm lines at the objective were 4.3 and 2.3 μW, respectively. The "Multi Track" option of the data acquisition software was used switching laser illumination line by line to minimize spectral crosstalk between the channels. Pixel time was 2.56 μs, and each line of the image was scanned four times and then averaged to reduce noise. The pinhole was set to 200 μm corresponding to an optical slice thickness of 1 μm. Images were collected from the middle plane of cells. The LSM data acquisition software was used to select ROIs including cells and to calculate the mean pixel intensities for each selected cell. FRET calculations with the mean intensities were performed with Microsoft Excel from $n \sim 100$–150 cells per sample. Average background intensities were determined from nontransfected cells. For pixel-by-pixel FRET calculations, the RiFRET plugin of the ImageJ software (37) was applied. Photobleaching was checked in a time lapse experiment. The intensity of ECFP and EYFP decreased by 0.1% and 0.6% between consecutive images.

Acceptor Photobleaching FRET on CLSM

Acceptor photobleaching FRET measurements were carried out on the Fos-Jun samples and the positive and negative controls with a Zeiss LSM 510 confocal microscope (Carl Zeiss, Jena, Germany). FRET efficiency results with the positive control (ECFP-EYFP fusion protein with a RNPPVAT-linker) were used as a reference for ratiometric FRET measurements with the different instruments. ECFP was excited by the 458-nm line of an Ar ion laser and detected between 465 and 510 nm; EYFP was excited at 514 nm and detected between 535 and 590 nm. First, images of the donor and acceptor distributions were taken. Then, acceptor dyes were bleached by repetitive scans with the 514-nm laser at maximal laser power. After photobleaching, a donor image was recorded again. The LSM data acquisition software was used to define ROIs and calculate the mean cellular fluorescence intensities in each channel. Mean cellular FRET efficiencies from the above mentioned intensities using formulas described in the Supporting Information were calculated in Microsoft Excel from $n > 20$ cells. In the calculations, corrections for incomplete acceptor bleaching, unwanted donor bleaching, crosstalk of acceptor, and acceptor photoproduct into the donor channel were taken into account (10). For details, see Supporting Information.

Data Analysis

Ratiometric Determination of FRET Efficiency

The calculation of ratiometric FRET efficiencies has been described earlier (38). Three signals (I_1: donor, I_2: transfer, and I_3: acceptor) were measured in independent channels from each cell or pixel. These intensities can be expressed as a function of the unquenched donor intensity (I_D), the acceptor intensity (I_A), the FRET efficiency (E), the spectral crosstalk (S_1–S_4), and fluorescence efficiency (α) factors:

$$\begin{aligned} I_1 &= I_D(1-E) + I_A S_4 + I_D E\alpha \frac{S_4}{S_2} \\ I_2 &= I_D(1-E) S_1 + I_A S_2 + I_D E\alpha \\ I_3 &= I_D(1-E) S_3 + I_A + I_D E\alpha \frac{\varepsilon_4}{S_2} \end{aligned} \tag{2}$$

All I_x fluorescence intensities in the equations are corrected for autofluorescence. Autofluorescence was determined using nontransfected cells. The spectral cross-talk factors S_1 and S_3 were calculated from cells expressing ECFP alone:

$$S_1 = \frac{I_2^D}{I_1^D} \qquad S_3 = \frac{I_3^D}{I_1^D} \tag{3 and 4}$$

For the confocal microscopic measurements, S_3 was negligible thanks to the filter set in channel 3 and the low excitability of ECFP at 514 nm. S_2 and S_4 were measured using cells expressing EYFP alone:

$$S_2 = \frac{I_2^A}{I_3^A} \qquad S_4 = \frac{I_1^A}{I_3^A} \tag{5 and 6}$$

Factor S_4 is negligible for the LSC because of the narrow band pass of the donor emission filter. To calculate S factors, the slopes of the appropriate intensity dot plots (e.g., I_2^D vs. I_1^D for S_1) were fitted with Deming's method (39) in Graphpad. The term ε_4 is a ratio of the extinction coefficients of ECFP and EYFP at the wavelengths used for exciting the donor and the acceptor. For the FACSAria and the LSC:

$$\varepsilon_4 = \frac{\varepsilon_{488}^{\mathrm{ECFP}}\, \varepsilon_{405}^{\mathrm{EYFP}}}{\varepsilon_{405}^{\mathrm{ECFP}}\, \varepsilon_{488}^{\mathrm{EYFP}}} \tag{7}$$

and for the CLSM:

$$\varepsilon_4 = \frac{\varepsilon_{514}^{\mathrm{ECFP}}\, \varepsilon_{458}^{\mathrm{EYFP}}}{\varepsilon_{458}^{\mathrm{ECFP}}\, \varepsilon_{514}^{\mathrm{EYFP}}} \tag{8}$$

The values of the extinction coefficients are given in Supporting Information Table S1; the value of ε_4 was negligible for the CLSM. The factor α, which is an "exchange rate" between donor and acceptor fluorescence, relates the I_2 signal arising from a given number of excited EYFP molecules to the I_1 signal from the same amount of excited ECFP molecules is defined by the following equation:

$$\alpha = \frac{Q_{\mathrm{EYFP}}\, \eta_{\mathrm{EYFP}}}{Q_{\mathrm{ECFP}}\, \eta_{\mathrm{ECFP}}}, \tag{9}$$

where Q_{ECFP} and Q_{EYFP} are the fluorescence quantum yields of ECFP and EYFP, and η_{ECFP} and η_{EYFP} are the detection

efficiencies (including emission filter transmissions, detector sensitivities, and amplifications) of ECFP and EYFP fluorescence emission in channels 1 and 2, respectively. The value of α can be determined from two samples expressing known amounts of ECFP or EYFP as:

$$\alpha = \frac{I_2^{\mathrm{EYFP}}}{I_1^{\mathrm{ECFP}}} \frac{N^{\mathrm{ECFP}}}{N^{\mathrm{EYFP}}} \varepsilon_2, \tag{10}$$

where I_1^{ECFP} and I_2^{EYFP} are the fluorescence intensities of ECFP and EYFP directly excited at the donor excitation wavelength

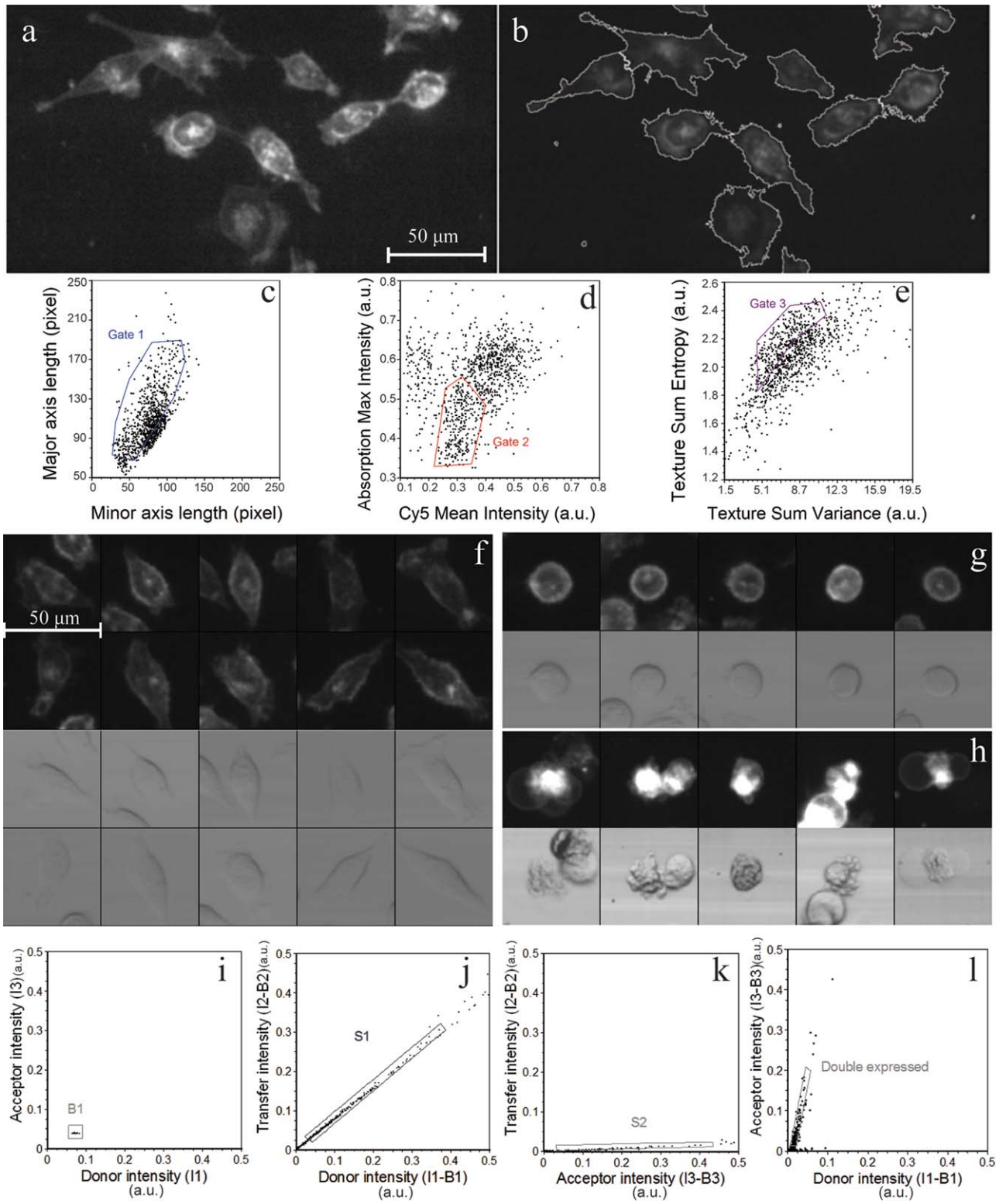

Figure .1

(405 for the FACSAria and the LSC and 458 nm for the confocal microscope), N^{ECFP}/N^{EYFP} is the ratio of ECFP and EYFP fluorophores expressed by the samples, and ε_2 is the ratio of their extinction coefficients at the donor excitation wavelength. For the FACSAria and the LSC:

$$\varepsilon_2 = \frac{\varepsilon_{405}^{ECFP}}{\varepsilon_{405}^{EYFP}} \tag{11}$$

and for the CLSM:

$$\varepsilon_2 = \frac{\varepsilon_{458}^{ECFP}}{\varepsilon_{458}^{EYFP}}. \tag{12}$$

Earlier, in our study, applying EGFP and mRFP1 as a FRET pair, α was determined with an iterative procedure using donor–acceptor fusion proteins of EGFP and mRFP1 (23). Here, we introduce a new method without iteration to calculate α using the ECFP-EYFP fusion protein expressing the fluorophores at a 1:1 ratio. The factor α can be expressed as:

$$\alpha = \frac{I_A S_2}{I_D}\varepsilon_2 \tag{13}$$

Equations (2) and (13) form a set of four equations with four unknowns (I_D, I_A, E, and α), which can be solved once the S factors have been determined with singly labeled cells. The solution for α is then

$$\alpha = \frac{S_2(I_1((1+\varepsilon_2)S_2S_3-(1+\varepsilon_2\varepsilon_4)S_1)-(1+\varepsilon_2)I_3(S_2-S_1S_4)+I_2(1-S_3S_4+\varepsilon_2(\varepsilon_4-S_3S_4)))}{(\varepsilon_4-1)(I_1S_2-I_2S_4)} \tag{14}$$

From the cell-by-cell, α values gained from Eq. (14), the average for the whole cell population of the ECFP-EYFP-transfected sample was calculated and was substituted into Eq. (2) for subsequent FRET analysis of the ECFP-EYFP and all the other doubly transfected samples. By using this new formula, we could get the value of the α factor in a single step in contrast to the previously applied iterative calculation (23). The FRET efficiency was expressed as

$$E = \frac{S_2(I_2-I_1S_1-I_3S_2+I_1S_2S_3+I_3S_1S_4-I_2S_3S_4)}{\alpha(1-\varepsilon_4)(I_1S_2-I_2S_4)+S_2(I_2-I_1S_1-I_3S_2+I_1S_2S_3+I_3S_1S_4-I_2S_3S_4)} \tag{15}$$

The other unknowns of Eq. (2): total unquenched donor fluorescence I_D and total acceptor fluorescence I_A can be calculated as:

$$I_D = \frac{\alpha(\varepsilon_4-1)(I_1S_2-I_2S_4)+S_2(I_1S_1+I_3S_2-I_1S_2S_3-I_3S_1S_4+I_2(S_3S_4-1))}{\alpha(\varepsilon_4-1)(S_2-S_1S_4)} \tag{16}$$

$$I_A = \frac{\varepsilon_4(I_2-I_1S_1)-I_3S_2+I_1S_2S_3+I_3S_1S_4-I_2S_3S_4}{(\varepsilon_4-1)(S_2-S_1S_4)} \tag{17}$$

In addition to the above parameters, the acceptor-to-donor expression ratio can also be calculated. First, the $Q = I_A/I_D$ acceptor-to-donor intensity ratio should be determined for the positive control (ECFP-EYFP) from Eqs. (16) and (17). For this fusion protein, the acceptor-to-donor expression ratio is 1. Then, the acceptor-to-donor protein expression ratio for a doubly transfected sample is:

$$\frac{N_A}{N_D} = \frac{I_A}{I_D Q} \tag{18}$$

Equation (2) and those describing E, I_D, I_A, and α are considerably simplified for the LSC and the confocal microscope (see Supporting Information) because of the negligible values of S_4 (LSC) or S_3 and ε_4 (confocal).

Results

Detection of Cells by Automatic Segmentation, Gating of Cellular Events, and FRET Analysis

Raw images captured by LSC were analyzed with CellProfiler, an open-source software developed for high-throughput analysis of imaging cytometry data (40). CellProfiler features auto-segmentation and declumping modules using Otsu's method (41). The Cy5 signal was used primarily to detect cellular events (Fig. 1a). Identified events were marked with contour lines surrounding the event (Fig. 1b). Cellular

Figure 1. Segmentation and multistep gating of LSC data. (**a** and **b**) CellProfiler image analysis software was applied, in which Otsu's auto-threshold module was used to detect cellular events and declump cell clusters that have distinctive Cy5 signal. Identified events were marked by segmentation contours (gray lines). (**c**) Adherent cells with elongated processes having a clear difference between the major and minor axes were selected in gate 1. (**d**) Floating cells having a large absorption signal and dead cells highly permeable to the Cy5 stain were excluded by gate 2. (**e**) Cells with granular morphology or blebbing membrane (suggestive of necrotic and apoptotic cells) were excluded by gate 3. (**f–h**) Galleries of randomly picked cells from the gated population were generated to visually confirm the outcome of the gating procedure. Typical attached (f), floating (g), and dead cells (h) are presented. (**i**) Background determination was done on single Cy5-labeled cells for auto-fluorescence correction. Cells in gate B1 were selected for determining background intensities of donor and acceptor signals; background of the transfer signal was determined similarly. (**j**) Background-corrected intensities of donor and transfer signals from the single ECFP-labeled sample were plotted to determine the *S*1 correction factor. (**k**) Similarly, transfer vs. acceptor signals from the single EYFP-labeled sample was used to determine *S*2. (**l**) From double-labeled samples, cells expressing both donor and acceptor (Fos-ECFP and Jun-EYFP) were selected for FRET evaluation. Highly overexpressing cells were excluded. [Color figure can be viewed in the online issue which is available at wileyonlinelibrary.com.]

Table 1. FRET efficiencies gained by confocal microscopy

	RATIOMETRIC E (MEAN ± SD) WITH ε_2=3.18	RATIOMETRIC E (MEAN ± SD) WITH ε_2=3.97	ACCEPTOR PHOTOBLEACHING E (MEAN ± SD)
ECFP-EYFP (positive control)	47.3 ± 3%	37.9 ± 2.5%	48.5 ± 1.8%
ECFP + EYFP (negative control)	0.9 ± 1.2%	0.6 ± 0.8%	1.0 ± 1.5%
Fos^{215}-ECFP + Jun-EYFP	22.0 ± 1.9%	16.0 ± 1.1%	21.2 ± 3.3%
Fos-ECFP + Jun-EYFP	7.9 ± 2.5%	5.5 ± 1.7%	8.0 ± 3.6%

Ratiometric calculations were carried out assuming ε_{434}^{CFP} = 26,000 M^{-1} cm^{-1} (left column) or 32,500 M^{-1} cm^{-1} (center column).

parameters within the contours: fluorescence intensity profiles, area, perimeter, circularity, and location parameters of the events were generated and displayed by the software. Events underwent a multistep gating procedure. First, cells having a clear difference between the lengths of the major and minor axes, assumedly being adherent and having long filopodia, were selected (Figs. 1c and 1f). Floating detached cells obviously featured rounded shape with equal axes (Figs. 1c and 1g). Cells having high absorption signals were generally necrotic or apoptotic and were excluded from FRET analysis. These cells usually had high mean Cy5 intensities also because of their highly permeable membrane, and possessed a more granular texture (Figs. 1d, 1e, and 1h). Cellular texture parameters "sum entropy" and "sum variance" were computed by a built-in module of CellProfiler. Sum entropy is a measure of randomness within an image, whereas variance increases as the variability of pixel intensity of an image is increased (42).

From gated cells of dot plots, a gallery of 100–150 randomly chosen cells was displayed. Visual observation confirmed that the gating strategy outlined above sufficiently discriminated between attached healthy and detached dead or dying cells (Figs. 1f–1h).

Background determination for autofluorescence correction was done on Cy5-labeled nontransfected cells (Fig. 1i). Dot plots of background-corrected mean pixel intensities I_2 vs. I_1 (Fig. 1j) or I_3 vs. I_1 intensities from single ECFP-transfected cells were plotted to determine the S_1 and S_3 correction factors as the slopes of these graphs. Similarly, I_2 vs. I_3 signals from single EYFP-transfected cells were used to determine S_2 (Fig. 1k). From double-labeled samples, cells expressing both donor and acceptor were selected for FRET evaluation (Fig. 1l). FRET efficiencies on a pixel-by-pixel or cell-by-cell basis were calculated using CellProfiler and Microsoft Excel, respectively, according to Eq. (S2) in the Supporting Information.

Ratiometric and Acceptor Photobleaching FRET Results Obtained by Confocal Microscopy

Confocal microscopic FRET measurements by the ratiometric (22,23) and acceptor photobleaching (10,43,44) techniques are well established. We used these techniques to determine FRET on a Zeiss LSM 510 confocal microscope. Results of cell-by-cell measurements for the positive and negative controls (ECFP-EYFP fusion, ECFP, and EYFP expressed as separate proteins) and for the full length and truncated Fos-Jun complexes are shown in Table 1. We used the acceptor bleaching FRET results as reference for the ratiometric values. The extent of heterodimer formation by Fos and Jun depends on the absolute concentrations as well as the relative amounts of these proteins: with increasing acceptor-to-donor ratio the FRET efficiency increases (23). Therefore, for comparing FRET efficiencies gained with the two methods, we selected those cells for which this ratio was higher than 1 and the E vs. acceptor-to-donor ratio curve had a plateau (Supporting Information Fig. S2). Full length Fos has a longer C terminal domain than Jun, whereas the C terminal domain of the truncated Fos^{215} after the dimerization domain is similar in length to that of Jun. Therefore, the FRET efficiency between Fos^{215}-Jun is significantly higher than for the full length Fos-Jun pair (23).

The laser lines of the microscope (458 and 514 nm) are optimal for the excitation of ECFP and EYFP, yielding an excellent signal-to-noise ratio. For calculating FRET efficiencies, knowledge of the α factor is indispensable. The excitability of EYFP at 458 nm is sufficiently high (ε_{458}^{EYFP} is 8.2% of the peak extinction) to allow for the reliable determination of the S_2 [Eq. (5)], ε_2 [Eq. (12)], and, via Eqs. (13) and (14), the α factors, making reliable FRET calculations possible. Two ratiometric FRET efficiency values are reported for each sample corresponding to two different values of the ε_2 absorption ratio. The reason for this uncertainty is the following. E is a monotonously decreasing function of the α factor [Eq. (15)], which itself depends linearly on ε_2, the ratio of the extinction coefficients of ECFP and EYFP at the donor excitation wavelength, 458 nm [Eqs. (12) and (13)]. Because there is ambiguity regarding the peak extinction coefficient of ECFP in the literature (ε_{434}^{ECFP} = 26,000 M^{-1} cm^{-1} in (45); 28,750 in (46); 32,500 in (47)), ε_2 cannot be determined unequivocally. The extinction coefficients of ECFP and EYFP at 458 nm (Supporting Information Table S1) were estimated as the product of the peak extinction coefficient of the corresponding dye and the extinction at 458 nm relative to the peak. The relative percentages were assessed from the excitation spectra of ECFP (measured in house on a Jobin Yvon Fluorolog 3 spectrofluorimeter) and EYFP (using the BD Fluorescence Spectrum Viewer on the Becton Dickinson homepage). As shown in Table 1, the FRET efficiency values determined by the ratiometric method are in good agreement with the acceptor photobleaching FRET results. We considered the FRET efficiencies from acceptor photobleaching experiments as reference values for the other techniques.

Ratiometric FRET Results Obtained by LSC and Flow Cytometry

To measure ratiometric FRET with high throughput, we used LSC and flow cytometry. As explained above, the major difficulty in ratiometric FRET calculations is the

Table 2. Ranges of possible extinction coefficient ratios and corresponding FRET efficiencies for the positive control sample gained by LSC or flow cytometry

	$\varepsilon_2 = \frac{\varepsilon_{405}^{CFP}}{\varepsilon_{405}^{YFP}}$	$\varepsilon_4 = \frac{\varepsilon_{488}^{CFP}\,\varepsilon_{405}^{YFP}}{\varepsilon_{405}^{CFP}\,\varepsilon_{488}^{YFP}}$	RANGE OF AVERAGE *E* FOR POSITIVE CONTROL (ECFP-EYFP)
Laser scanning cytometer	42.6–9.5	0.0029–0.0066	44%–224%
Flow cytometer			31%–135%

determination of the α factor [Eq. (13)], for which knowledge of the ε_2 and the S_2 factors are required. In the case of the LSC and the flow cytometer, the 405 and 488 nm laser lines were used to excite ECFP and EYFP, respectively. ε_2 depends linearly on ε_{405}^{EYFP}, which is less than 2% of the peak extinction value (Supporting Information Table S1), and its exact value is not known. In addition, S_2 is determined from I_2^A, the acceptor fluorescence excited at 405 nm, which is very low due to the low extinction coefficient. Therefore, the value of both of these parameters (and consequently α), carries large error, and leads to a large uncertainty of *E* values. A further source of error is the uncertainty in ε_4 [Eq. (7)], which also depends on ε_{405}^{EYFP}. When substituting the possible extreme values of ε_{405}^{EYFP} and ε_{405}^{ECFP} (Supporting Information Table S1) into the expressions of ε_2 and ε_4, the resulting ranges of *E* values for the positive control are very broad (Table 2). The uncertainty of the extinction coefficients involved in the equations impairs quantitative FRET calculations. To get around this problem, we used the FRET efficiency of the positive control from acceptor photobleaching ($E = 48.5\%$) as a standard. The utility of this sample as a standard is that it has an intramolecular FRET process; thus, the FRET efficiency is independent of the expression level of the ECFP-EYFP protein. In the FRET calculations of LSC, flow cytometric and confocal microscopic data according to Eq. (15) the value of α was set to yield $E = 48.5\%$ for the population average. This α was used in subsequent FRET calculations of the Fos-Jun samples and the negative control. By using this approach, FRET efficiencies derived from the different instruments show excellent agreement (Table 3).

In addition to being able to measure a large number of cells, LSC has the advantage that it can also provide a map of subcellular FRET distribution. Thus, protein–protein interactions can be localized to specific cellular compartments. Such FRET efficiency maps of Fos-Jun interactions are shown (Fig. 2) along with similar data gained by confocal microscopy (Fig. 3). Fos-Jun dimers show nuclear localization, whereas the positive and negative controls are present in the whole cell. Pixel-by-pixel FRET efficiencies from the two instruments are nearly identical and show no significant spatial variation, similar to earlier results on Fos and Jun pairs (23). The advantage of confocal FRET images is their higher optical resolution (limit of resolution: r∼230 nm) and better signal-to-noise ratio, whereas LSC provides higher throughput with somewhat lower resolution (r∼420 nm).

A pipeline exemplifying the gating and FRET analysis procedure using the CellProfiler software has been made accessible at our web site (http://biophys.med.unideb.hu/en/node/227).

Discussion

FRET has a renaissance of biomedical applications, where its capacity to indicate molecular proximity relations is used. A major field of application is the screening of protein–protein interactions, which is important in many areas of biological research such as the study of signaling pathways or drug discovery. Recently, high throughput assays applying microscopic techniques with TIRF illumination to detect membrane protein interactions (48), or interactions between cells attached to a micropatterned surface with a "prey" protein (49) have been reported. FRET measured by fluorescence lifetime imaging microscopy has been applied to quantify post-translational modifications in live cells (50) in a high throughput fashion. Here, we worked out a simple procedure to collect and analyze FRET data in a semiautomated fashion by using a commercially available laser scanning cytometer with a typical three-laser setup and open-source software. Raw images collected with the own software of the LSC were processed with the Cell Profiler open source image analysis program according to a custom protocol developed by us. In this procedure adherent, healthy cells expressing the protein of interest in sufficiently high amounts were selected and the cell-by-cell fluorescence intensities necessary for FRET analysis were calculated. Actual FRET calculations can be performed in any spreadsheet program using the classic ratiometric FRET equations. The throughput of FRET data acquisition by LSC (60 cells/min) was between that of confocal microscopy (1 cell/min) and flow cytometry (50,000 cells/min). The total data acquisition time for a complete FRET experiment by LSM with FRET samples and controls (50 cells/sample) took 6 h and the data analysis 4 h. For LSC, acquisition (3000 cells/

Table 3. FRET efficiencies calculated on a cell-by-cell basis with α factors set to yield E = 48.5% for the positive control, the standard E value from acceptor photobleaching FRET

SAMPLE	CONFOCAL LASER SCANNING MICROSCOPE *E* (MEAN ± SD)	LASER SCANNING CYTOMETER *E* (MEAN ± SD)	FLOW CYTOMETER *E* (MEAN ± SD)
ECFP-EYFP (positive control)	48.5%	48.5%	48.5%
ECFP + EYFP (negative control)	0.84 ± 0.9%	0.65 ± 1.6%	1.8 ± 1%
Fos^{215}-ECFP + Jun-EYFP	21.1 ± 1.3%	23.6 ± 2.8%	22.1 ± 3.7%
Fos-ECFP + Jun-EYFP	8.3 ± 1.9%	8.6 ± 2.9%	10.2 ± 3.6%

E values were calculated only for cells with an acceptor-to-donor ratio larger than 1.

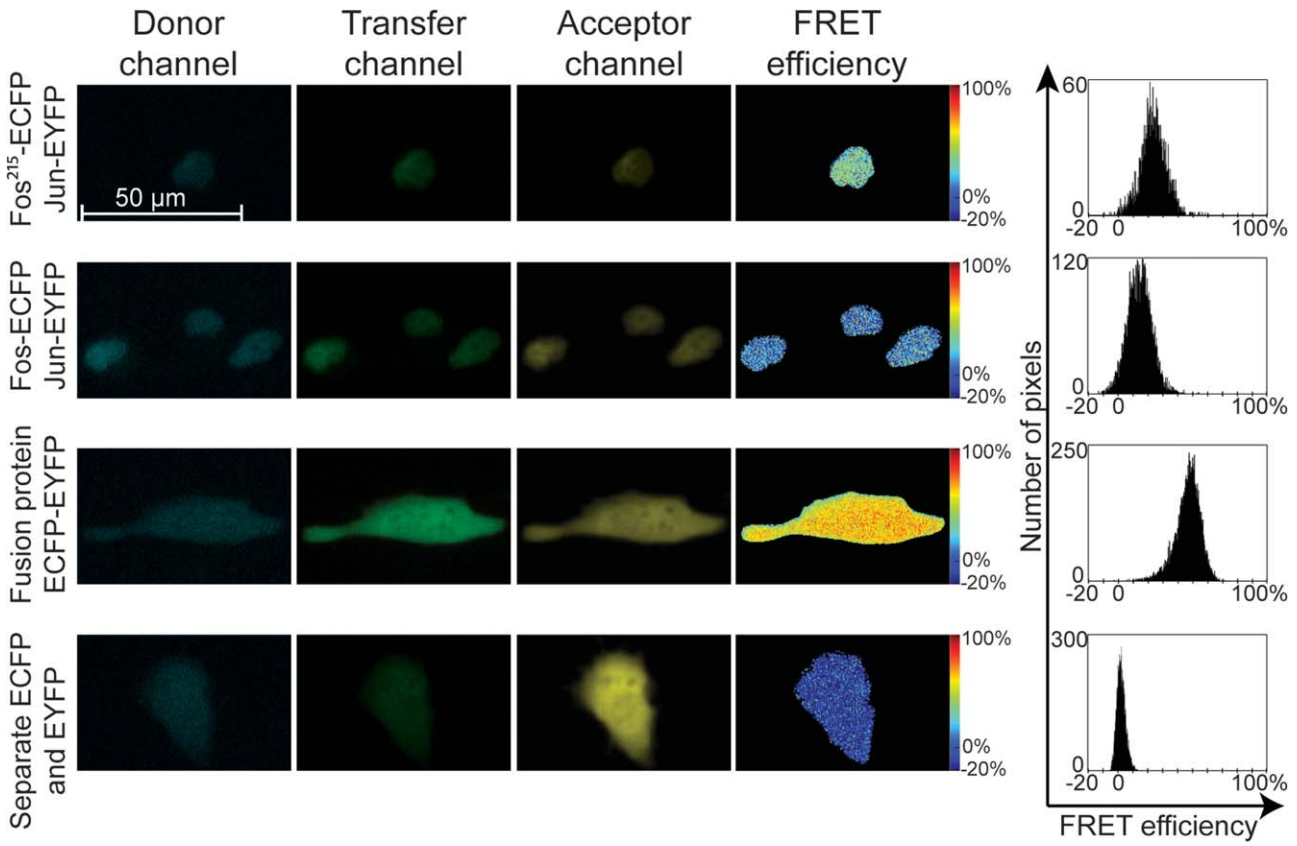

Figure 2. Pixel-by-pixel FRET analysis of LSC images. FRET experiments carried out on the laser scanning cytometer. ECFP (blue) was excited at 405 nm and detected between 460 and 500 nm; in the transfer channel (green), excitation was performed at 405 nm and detected between 520 and 580 nm; EYFP (yellow) was excited at 488 nm and detected between 520 and 580 nm. Fos215-ECFP + Jun-EYFP (top row) and full length Fos-ECFP + Jun-EYFP (second row) showed nuclear localization with mean $E = 23.6\%$ and 8.6%; the positive control, ECFP-EYFP, and the negative control, ECFP and EYFP, expressed independently (third and fourth rows) were evenly distributed in the whole cell and yielded averages of $E = 48.5\%$ and 2.1%. From these signals, the FRET efficiency was calculated in each pixel and its subcellular distribution was displayed as a FRET efficiency false color image. Pixel-by-pixel E values were also presented as frequency distribution histograms. [Color figure can be viewed in the online issue which is available at wileyonlinelibrary.com.]

sample) took 4 h, and did not require the presence of the operator, whereas analysis required 0.5 h/sample. FACS data acquisition and analysis took 2 h and 1 h, respectively.

ECFP and EYFP are among the most frequently used FRET reporters thanks to the ease at which they can be expressed as fusion proteins, and their significant spectral overlap resulting in a large Förster distance (4.92 ± 0.1 nm (20)). In ratiometric FRET calculations, a pivotal element of the analysis is the determination of the α factor, which relates the signals arising from equal amounts of excited donor and acceptor molecules to each other. When calculating α, the donor and acceptor fluorescence intensities must be normalized by the number of molecules and by the efficiency of excitation. It is practical to use donor–acceptor fusion proteins, in which the donor and acceptor dyes are present at a 1:1 ratio. Normalization by the excitation efficiency is usually achieved by applying the same laser line to excite the donor and the acceptor, and division of the resulting fluorescence intensities by the ratio of the extinction coefficients of the two dyes at this wavelength (ε_2). For the ECFP-EYFP pair, the 458 nm line is optimal for exciting ECFP, and sufficient to excite EYFP (Supporting Information Table S1). Because not all instruments have the optimal wavelengths for all possible dye pairs, it may be necessary to measure a reference sample at its optimal excitation wavelengths on another instrument. Its E value may then serve as a standard. The 458 and 514 lines are not available in the LSC and the BD FACSAria flow cytometer used in our study. The 405 nm line is suitable for exciting ECFP (the extinction coefficient is 55.1% of the maximum). On the other hand, the extinction of EYFP at this wavelength is very low; thus, α cannot be defined precisely. As a reference sample, we used an ECFP-EYFP fusion protein with a high E, which can be measured reproducibly, and is independent of the expression level. We demonstrated that using a FRET standard with predetermined FRET efficiency makes the determination of the α factor and reliable FRET measurements possible when using the 405 and 488 nm lasers. This was confirmed by the good agreement between results gained by acceptor photobleaching and ratiometric FRET techniques with the different instruments. By the application of the FRET standard, the FRET efficiency differences between the full-length Fos-ECFP + Jun-EYFP and the truncated Fos^{215}-

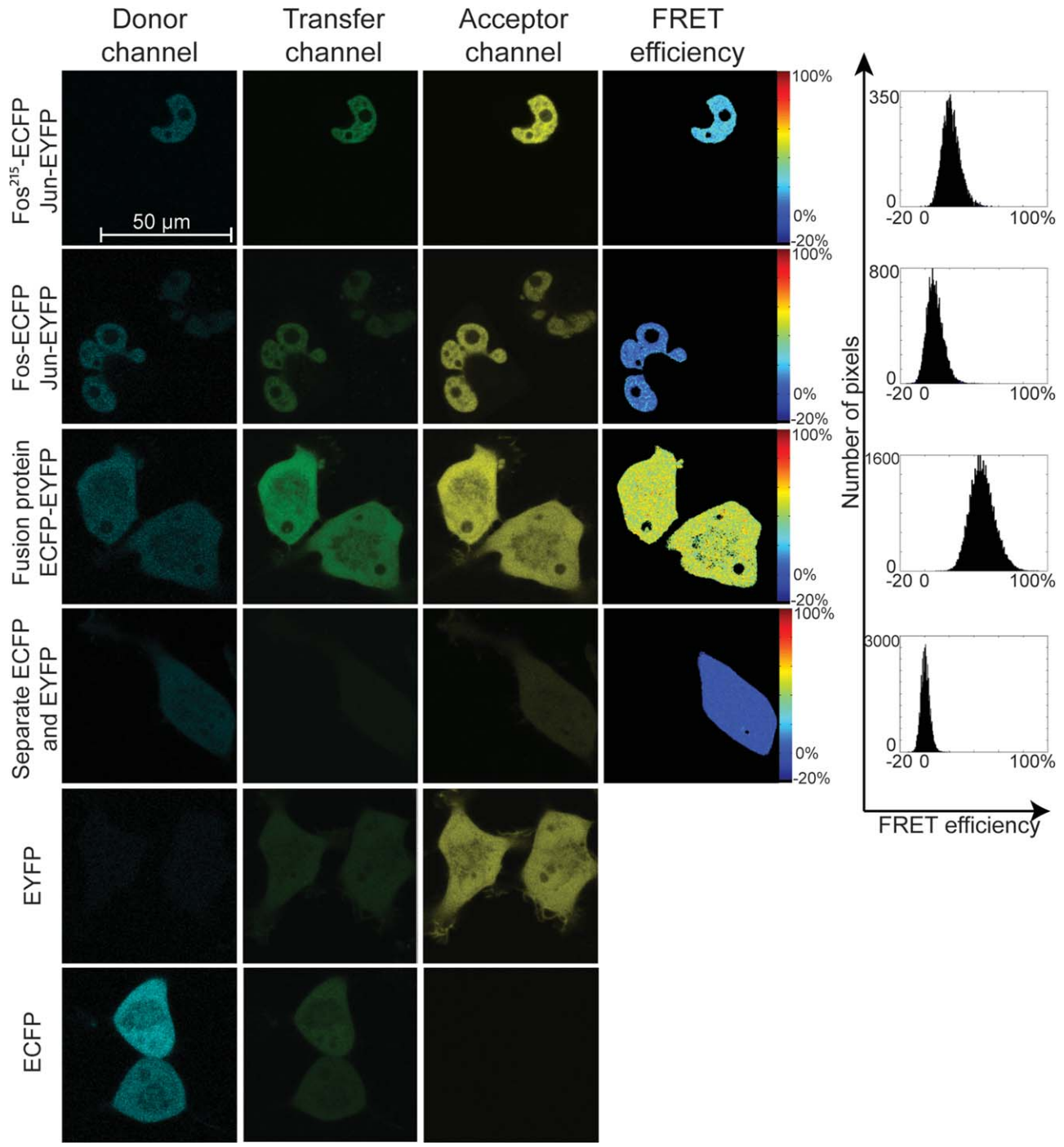

Figure 3. Pixel-by-pixel FRET analysis of confocal microscopic images. FRET experiments on HeLa cells using a Carl Zeiss LSM510 confocal microscope. ECFP (blue) was excited with the 458 nm line of an Ar ion laser and detected between 475 and 525 nm; in the transfer channel (green), excitation occurred at 458 nm and detection between 530 and 600 nm; EYFP (yellow) was excited at 514 nm and detected between 530 and 600 nm. Mean *E* values were: 21.1% for Fos215-ECFP + Jun-EYFP, 8.3% for Fos-ECFP + Jun-EYFP, 48.5% for the positive, and 0.1% for the negative control ($n \sim 20$ cells/sample).

ECFP + Jun-EYFP protein pairs could clearly and reproducibly be resolved with all three methods. We also carried out pixel-by-pixel FRET analysis of LSC and confocal microscopic images, which yielded identical FRET distributions with each other and with the results of cell-by-cell analysis. This gives evidence that the sensitivity of LSC is sufficient for subcellular FRET analysis as well.

The interpretation of the measured apparent FRET efficiencies is complicated by the existence of multiple photophysical states of the dyes, the unknown relative orientation of

the transition dipoles of the dyes (51) and the variable extent of association between the donor- and acceptor-labeled molecules. ECFP and EYFP are characterized by at least two lifetimes each, and EYFP may be in a nonabsorbing dark state, which does not function as a FRET acceptor. Therefore, three lifetimes were discerned for an ECFP-EYFP fusion protein indicating that different donor–acceptor configurations were present characterized by distinct FRET efficiencies (52). Thus, apparent FRET efficiencies by intensity based FRET (including acceptor bleaching and ratiometric methods) are averages of real FRET efficiencies of the different species. In the case of intermolecular FRET, incomplete association of donor- and acceptor-labeled molecules results in a decreased apparent FRET efficiency. Titration of the acceptor-to-donor ratio (23) showed that at high A-to-D ratios the apparent *E* reached a saturation value (see Supporting Information), which can be regarded as the value characterizing the fully associated state. Thus, useful comparisons can be made between different conformations of complexes or different association states of donor- and acceptor-labeled molecules using ratiometric measurements.

Our data exemplify that FRET can be used as an additional modality in the versatile, high throughput analysis of cells by LSC. Such analyses could yield important information on molecular interactions not available by methods previously used in LSC.

Acknowledgments

We thank Drs. Dániel Beyer and György Vereb for comparing their acceptor photobleaching FRET data with ours and Attila Forgács for calculating confocal microscopic pixel-by-pixel FRET histograms.

Literature Cited

1. Förster T. Energiewanderung und Fluoreszenz. Die Naturwissenschaften 1946;6:166–175.
2. Clegg RM. Fluorescence resonance energy transfer. Curr Opin Biotechnol 1995;6:103–110.
3. Szöllösi J, Damjanovich S, Nagy P, Vereb G, Mátyus L. Principles of resonance energy transfer. In: Robinson JP, editor. Current Protocols in Cytometry, Chapter 1. Hoboken, NJ: John Wiley & Sons; 2006. Unit 1.12.
4. Stryer L. Fluorescence energy transfer as a spectroscopic ruler. Annu Rev Biochem 1978;47:819–846.
5. Szöllösi J, Damjanovich S, Mátyus L. Application of fluorescence resonance energy transfer in the clinical laboratory: Routine and research. Cytometry 1998;34:159–179.
6. Jares-Erijman EA, Jovin TM. FRET imaging. Nat Biotechnol 2003;21:1387–1395.
7. Jovin TM, Arndt-Jovin DJ. Luminescence digital imaging microscopy. Annu Rev Biophys Biophys Chem 1989;18:271–308.
8. Szentesi G, Vereb G, Horváth G, Bodnár A, Fábián Á, Matkó J, Gáspár R, Damjanovich S, Mátyus L, Jenei A. Computer program for analyzing donor photobleaching FRET image series. Cytometry Part A 2005;67A:119–128.
9. Bastiaens PI, Majoul IV, Verveer PJ, Soling HD, Jovin TM. Imaging the intracellular trafficking and state of the AB5 quaternary structure of cholera toxin. EMBO J 1996;15:4246–4253.
10. Roszik J, Szöllösi J, Vereb G. AccPbFRET: An ImageJ plugin for semi-automatic, fully corrected analysis of acceptor photobleaching FRET images. BMC Bioinformatics 2008;9:346–351.
11. Tron L, Szollosi J, Damjanovich S. Flow cytometric measurement of fluorescence resonance energy transfer on cell surfaces. Quantitative evaluation of the transfer efficiency on a cell-by-cell basis. Biophys J 1984;45:939–946.
12. Takanishi CL, Bykova EA, Cheng W, Zheng J. GFP-based FRET analysis in live cells. Brain Res 2006;1091:132–139.
13. Vereb G, Matkó J, Szöllösi J. Cytometry of fluorescence resonance energy transfer. Methods Cell Biol 2004;75:105–152.
14. Vámosi G, Vereb G, Bodnár A, Tóth K, Baudendistel N, Damjanovich S, Szöllősi J. Fluorescence-resonance energy transfer (FRET). In: Sack U, Tarnok A, Rothe G, editors. Cellular Diagnostics. Germany: Karger, 2009. p 738.
15. Tramier M, Zahid M, Mevel JC, Masse MJ, Coppey-Moisan M. Sensitivity of CFP/YFP and GFP/mCherry pairs to donor photobleaching on FRET determination by fluorescence lifetime imaging microscopy in living cells. Microsc Res Tech 2006;69:933–939.
16. Domingo B, Sabariegos R, Picazo F, Llopis J. Imaging FRET standards by steady-state fluorescence and lifetime methods. Microsc Res Tech 2007;70:1010–1021.
17. Chen YC, Spring BQ, Clegg RM. Fluorescence lifetime imaging comes of age how to do it and how to interpret it. Methods Mol Biol 2012;875:1–22.
18. Gansen A, Hauger F, Tóth K, Langowski J. Single-pair fluorescence resonance energy transfer of nucleosomes in free diffusion: Optimizing stability and resolution of subpopulations. Anal Biochem 2007;368:193–204.
19. Gansen A, Valeri A, Hauger F, Felekyan S, Kalinin S, Toth K, Langowski J, Seidel CA. Nucleosome disassembly intermediates characterized by single-molecule FRET. Proc Natl Acad Sci USA 2009;106:15308–15313.
20. Patterson GH, Piston DW, Barisas BG. Forster distances between green fluorescent protein pairs. Anal Biochem 2000;284:438–440.
21. He L, Olson DP, Wu X, Karpova TS, McNally JG, Lipsky PE. A flow cytometric method to detect protein-protein interaction in living cells by directly visualizing donor fluorophore quenching during CFP–>YFP fluorescence resonance energy transfer (FRET). Cytometry Part A 2003;55A:71–85.
22. Nagy P, Bene L, Hyun WC, Vereb G, Braun M, Antz C, Paysan J, Damjanovich S, Park JW, Szöllösi J. Novel calibration method for flow cytometric fluorescence resonance energy transfer measurements between visible fluorescent proteins. Cytometry Part A 2005;67A:86–96.
23. Vámosi G, Baudendistel N, von der Lieth C-W, Szalóki N, Mocsár G, Müller G, Brázda P, Waldeck W, Damjanovich S, Langowski J, et al. Conformation of the c-Fos/c-Jun complex in vivo: A combined FRET, FCCS, and MD-modeling study. Biophys J 2008;94:2859–2868.
24. Renz M, Daniels BR, Vámosi G, Arias IM, Lippincott-Schwartz J. Plasticity of the asialoglycoprotein receptor deciphered by ensemble FRET imaging and single-molecule counting PALM imaging. Proc Natl Acad Sci USA 2012;109:E2989–E2997.
25. Curran T, Franza BR Jr. Fos and jun: The AP-1 connection. Cell 1988;55:395–397.
26. Baudendistel M, Müller G, Waldeck W, Angel P, Langowski J. Two-hybrid fluorescence cross-correlation spectroscopy detects protein-protein interactions in vivo. ChemPhysChem 2005;6:984–990.
27. Kamentsky LA, Kamentsky LD. Microscope-based multiparameter laser scanning cytometer yielding data comparable to flow cytometry data. Cytometry 1991;12:381–387.
28. Darzynkiewicz Z, Bedner E, Li X, Gorczyca W, Melamed MR. Laser-scanning cytometry: A new instrumentation with many applications. Exp Cell Res 1999;249:1–12.
29. Pina-Vaz C, Costa-Oliveira S, Rodrigues AG, Salvador A. Novel method using a laser scanning cytometer for detection of mycobacteria in clinical samples. J Clin Microbiol 2004;42:906–908.
30. Bedner E, Melamed MR, Darzynkiewicz Z. Enzyme kinetic reactions and fluorochrome uptake rates measured in individual cells by laser scanning cytometry. Cytometry 1998;33:1–9.
31. Bacso Z, Eliason JF. Measurement of DNA damage associated with apoptosis by laser scanning cytometry. Cytometry 2001;45:180–186.
32. Kwon J. A new approach for the analysis of testicular cells using a laser scanning cytometer. Exp Anim 2006;55:483–486.
33. Mital J, Schwarz J, Taatjes DJ, Ward GE. Laser scanning cytometer-based assays for measuring host cell attachment and invasion by the human pathogen Toxoplasma gondii. Cytometry Part A 2006;69A:13–19.
34. Mittag A, Lenz D, Bocsi J, Sack U, Gerstner AO, Tarnok A. Sequential photobleaching of fluorochromes for polychromatic slide-based cytometry. Cytometry Part A 2006;69A:139–141.
35. Luther E, Darzynkiewicz Z, Barteneva N. Automated laser scanning imaging cytometry in apoptotic pathway characterization. Cambridge, MA: CompuCyte Corporation. 2004. Available at: http://www.compucyte.com/Application_Links/Automated%20Laser%20Scanning%20Imaging%20Cytometer%20in%20Apoptotic%20Pathway%20Characterization-8060003.pdf.
36. Szentesi G, Horváth G, Bori I, Vámosi G, Szöllösi J, Gáspár R, Damjanovich S, Jenei A, Mátyus L. Computer program for determining fluorescence resonance energy transfer efficiency from flow cytometric data on a cell-by-cell basis. Comput Methods Programs Biomed 2004;75:201–211.
37. Roszik J, Lisboa D, Szöllösi J, Vereb G. Evaluation of intensity-based ratiometric FRET in image cytometry—Approaches and a software solution. Cytometry Part A 2009;75A:761–767.
38. Sebestyen Z, Nagy P, Horvath G, Vamosi G, Debets R, Gratama JW, Alexander DR, Szöllösi J. Long wavelength fluorophores and cell-by-cell correction for autofluorescence significantly improves the accuracy of flow cytometric energy transfer measurements on a dual-laser benchtop flow cytometer. Cytometry 2002;48:124–135.
39. Linnet K. Estimation of the linear relationship between the measurements of two methods with proportional errors. Stat Med 1990;9:1463–1473.
40. Carpenter AE, Jones TR, Lamprecht MR, Clarke C, Kang IH, Friman O, Guertin DA, Chang JH, Lindquist RA, Moffat J, et al. CellProfiler: Image analysis software for identifying and quantifying cell phenotypes. Genome Biol 2006;7:R100.
41. Sezgin M, Sankur B. Survey over image thresholding techniques and quantitative performance evaluation. J Electron Imaging 2004;13:146–168.

42. Park B, Chen YR. Co-occurrence matrix texture features of multi-spectral images on poultry carcasses. J Agric Eng Res 2001;78:127–139.
43. Vámosi G, Bodnár A, Vereb G, Jenei A, Goldman CK, Langowski J, Tóth K, Mátyus L, Szöllosi J, Waldmann TA, et al. IL-2 and IL-15 receptor α-subunits are coexpressed in a supramolecular receptor cluster in lipid rafts of T cells. Proc Natl Acad Sci USA 2004;101:11082–11087.
44. Fazekas Z, Petrás M, Fábián Á, Pályi-Krekk Z, Nagy P, Damjanovich S, Vereb G, Szöllosi J. Two-sided fluorescence resonance energy transfer for assessing molecular interactions of up to three distinct species in confocal microscopy. Cytometry Part A 2008;73A:209–219.
45. Patterson G, Day RN, Piston D. Fluorescent protein spectra. J Cell Sci 2001;114:837–838.
46. Karasawa S, Araki T, Nagai T, Mizuno H, Miyawaki A. Cyan-emitting and orange-emitting fluorescent proteins as a donor/acceptor pair for fluorescence resonance energy transfer. Biochem J 2004;381:307–312.
47. Olympus FluoView Resource Center homepage. Available at: http://www.olympus-confocal.com/applications/fpcolorpalette.html.
48. Paar C, Paster W, Stockinger H, Schutz GJ, Sonnleitner M, Sonnleitner A. High throughput FRET screening of the plasma membrane based on TIRFM. Cytometry Part A 2008;73A:442–450.
49. Schwarzenbacher M, Kaltenbrunner M, Brameshuber M, Hesch C, Paster W, Weghuber J, Heise B, Sonnleitner A, Stockinger H, Schutz GJ. Micropatterning for quantitative analysis of protein-protein interactions in living cells. Nat Methods 2008;5:1053–1060.
50. Grecco HE, Roda-Navarro P, Fengler S, Bastiaens PI. High-throughput quantification of posttranslational modifications in situ by CA-FLIM. Methods Enzymol 2011; 500:37–58.
51. Ivanov V, Li M, Mizuuchi K. Impact of emission anisotropy on fluorescence spectroscopy and FRET distance measurements. Biophys J 2009;97:922–929.
52. Millington M, Grindlay GJ, Altenbach K, Neely RK, Kolch W, Benčina M, Read ND, Jones AC, Dryden DTF, Magennis SW. High-precision FLIM-FRET in fixed and living cells reveals heterogeneity in a simple CFP-YFP fusion protein. Biophys Chem 2007;127:155–164.